REPORT DOCUMENTATION PAGE

Public reporting burden for this collection of information is estimated to average 1 hour per response, including the time for reviewing instructions, searching existing data sources, gathering and maintaining the data needed, and completing and reviewing the collection of information. Send comments regarding this burden estimate or any other aspect of this collection of information, including suggestions for reducing this burden, to Washington Headquarters Services, Directorate for information Operations and Reports, 1215 Jefferson Davis Highway, Suite 1204, Arlington, VA 22202-4302, and to the office of Management and Budget, Paperwork Reduction Project (0704-0188), Washington, DC 20503.

1. AGENCY USE ONLY *(Leave blank)*	2. REPORT DATE June 2002	3. REPORT TYPE AND DATES COVERED Final Technical (07/01/98 - 12/31/01)

4. TITLE AND SUBTITLE "High Power Broadband Amplifiers for 1-18 GHz Naval Radar"	5. FUNDING NUMBERS N00014-98-1-0750
6. AUTHOR(S) Dr. Mark Rodwell / Dr. Umesh K. Mishra	

7. PERFORMING ORGANIZATION NAME(S) AND ADDRESS(ES) University of California, Santa Barbara, CA 93106	8. PERFORMING ORGANIZATION REPORT NUMBER

9. SPONSORING/MONITORING AGENCY NAME(S) AND ADDRESS(ES) Office of Naval Research Program Officer John C. Zolper ONR 312 800 North Quincy Street Arlington, VA 22217-5660	10. SPONSORING/MONITORING AGENCY REPORT NUMBER

11. SUPPLEMENTARY NOTES

12a. DISTRIBUTION/AVAILABILITY STATEMENT

Distribution Unlimited, approved for public release.

20020701 071

13. ABSTRACT *(Maximum 200 words)*

Three generations of dual-gate AlGaN/GaN HEMTs on sapphire were fabricated and characterized. First generation dual-gate HEMT had equal gate lengths of 650 nm produced through stepper lithography. Current gain cut-off frequency (ft) of 20 GHz, 60 V breakdown, 11 dB small-signal gain, 2.5 W/mm saturated output power, and 35% power added efficiency (PAE) at 4 GHz were achieved. Second and third generation dual-gate HEMT had unequal gate lengths to simultaneously achieve both large ft and breakdown voltage. Gate one located closest to the source had a gate length of 150 nm and gate two had a gate length of 300 nm. Both gates had "T" shaped cross-sections to reduce gate resistance and were defined by e-beam lithography. An ft of 52 GHz and breakdown voltage greater than 100 V was achieved for second generation dual-gate devices. Single gate devices with gate lengths of 150 nm fabricated on the same sample showed a breakdown voltage of 40 V. With an improvement in both gate lithography and material, third generation dual-gate devices produced an ft of 65 GHz, breakdown voltage of 70 V, 12 dB small-signal gain, 3.5 W/mm saturated output power, and 45% PAE at 8.2 GHz.

14. SUBJECT TERMS AlGaN/GaN, Dual-gate FETs, High breakdown			15. NUMBER OF PAGES 32
			16. PRICE CODE

17. SECURITY CLASSIFICATION OF REPORT UNCLASSIFIED	18. SECURITY CLASSIFICATION OF THIS PAGE UNCLASSIFIED	19. SECURITY CLASSIFICATION OF ABSTRACT UNCLASSIFIED	20. LIMITATION OF ABSTRACT UL

Final Report: Dual-Gate AlGaN/GaN Modulation-Doped Field-Effect Transistors

Abstract- Over the course of the program, three generations of dual-gate AlGaN/GaN HEMTs on sapphire have been fabricated and characterized. First generation dual-gate HEMT had equal gate lengths of 0.65 μm produced through stepper lithography. Current gain cut-off frequency (f_τ) of 20 GHz, 60 V breakdown, 11 dB small-signal gain, 2.5 W/mm saturated output power, and 35 % power added efficiency (PAE) at 4 GHz were achieved. Second generation dual-gate HEMT had unequal gate lengths to simultaneously achieve both large f_τ and breakdown voltage. Gate one located closest to the source had a gate length (L_{G1}) of 0.15 μm and gate two had a gate length (L_{G2}) of 0.3 μm. Both gates had "T" shaped cross-sections to reduce gate resistance and were defined by e-beam lithography. An f_τ of 52 GHz and breakdown voltage greater than 100 V was achieved. Single gate devices with gate lengths of 0.15 μm fabricated on the same sample showed a breakdown voltage of 40 V. Third generation dual-gate HEMT also had L_{G1} = 0.15 μm and L_{G2} = 0.3 μm, but an improvement in both gate lithography and material produced an f_τ of 65 GHz and a breakdown voltage of 70 V. Single gate devices with gate lengths of 0.15 μm fabricated on the same sample showed a breakdown voltage of 35 V. Third generation dual-gate HEMT achieved 12 dB small-signal gain, 3.5 W/mm saturated output power, and 45 % PAE at 8.2 GHz.

INTRODUCTION

Amplifiers operating over a decade bandwith while providing tens to hundreds of watts with high power added efficiency are needed for 2-20 GHz phased array radars currently in development. AlGaN/GaN-based transistors exhibit large breakdown voltages (V_{br}) that enable large amounts of power ($P_{out} \leq V_{br}^2/8R_L$) for high power electronics. An output power of 9.8 W/mm at 8.0 GHz has been demonstrated on SiC substrate [1] and a cutoff frequency, f_τ greater than 110 GHz has also been achieved with a gate-length of less than 0.1 μm [2].

For broadband common-source power amplifiers, the gain bandwidth product is limited to approximately f_τ. Increased f_τ can be obtained by reducing the gate length L_G, however the breakdown voltage V_{br} will be significantly reduced. In the Johnson limit [3], the product of $V_{br}f_\tau$ is less than $E_{max}v_{sat}/\pi$, where E_{max} and v_{sat} are the breakdown field and the electron velocity. Therefore, increased V_{br} is obtained at the expense of f_τ and high power levels are obtained at the expense of reduced amplifier bandwidth.

AlGaN/GaN dual-gate devices have the potential of simultaneously realizing a high f_τ and a high breakdown voltage. Moreover, smaller feedback capacitance and higher output impedance of dual-gate devices enable flexibility for circuit application of broadband power amplifiers. A dual-gate device is electrically equivalent to a common-source (CS)/common-gate (CG) cascode pair, but occupies less die area. The current gain of the dual-gate device, $h_{21}(jf) = (f_{\tau 1}/jf)(1 + jf/f_{\tau 2})^{-1}$, deviates from that of the

CS device $h_{21}(jf) = (f_{\tau 1}/jf)$ for $f > f_{\tau 2}$, where $f_{\tau 1}$ and $f_{\tau 2}$ are the current gain cutoff frequencies of the CS and CG devices and f is the signal frequency. To provide substantial current gain, $f_{\tau 1}$ must be several times of the signal frequency f. In contrast, to avoid significant loss (i.e., >10 %) in h_{21} in the CG stage, it is sufficient to have $f_{\tau 2}$ of $1.5f$ to $2f$. The breakdown voltage is however determined by the CG device. Therefore, in a dual-gate device, it is advantageous to design the CS device with short L_g hence high f_τ and the CG device with long L_g hence lower f_τ but improved V_{br}. High bandwidth and high power are thus simultaneously obtained.

MATERIAL STRUCTURE

The epilayers of $Al_{0.3}Ga_{0.7}N/GaN$ dual-gate devices were grown by metal organic chemical vapor deposition (MOCVD) on a c-plane sapphire substrate. The material structure began with a 200 Å thick GaN nucleation layer, followed by 3 µm thick insulating i-GaN as a device buffer layer. The $Al_{0.3}Ga_{0.7}N$ contains a 30 Å unintentionally doped spacer layer, a 120 Å Si-doped charge supply layer and a 50 Å thick cap layer. Typical sheet electron concentrations and electron Hall mobilities of as-grown wafers were ~1.0×10^{13} cm^{-2} and 1,200 cm^2/V-s at room temperature.

FIRST GENERATION DUAL-GATE ALGAN/GAN HEMT

First generation dual-gate HEMT had equal gate lengths of 0.65 µm produced through stepper lithography. Capacitors to ground the gate of the CG device were fabricated with a 1000Å thick SiO_2 on the source contacts (~125 µm x 90 µm). The first gate was separated by 0.7 µm from the source and by 1.5 µm from the second gate. Current gain cut-off frequency (f_τ) of 20 GHz, 60 V breakdown, 11 dB small-signal gain, 2.5 W/mm saturated output power, and 35 % power added efficiency (PAE) at 4 GHz were achieved. All relevant plots are contained in the Power Point presentation that is attached.

SECOND GENERATION DUAL-GATE ALGAN/GAN HEMT

Second generation dual-gate HEMT had unequal gate lengths to simultaneously achieve both large f_τ and breakdown voltage. Gate one located closest to the source had a gate length (L_{G1}) of 0.15 µm and gate two had a gate length (L_{G2}) of 0.3 µm. Both gates had "T" shaped cross-sections to reduce gate resistance and were defined by e-beam lithography. An f_τ of 52 GHz and breakdown voltage greater than 100 V was achieved. Single gate devices with gate lengths of 0.15 µm fabricated on the same sample showed a breakdown voltage of 40 V. All relevant plots are contained in the Power Point presentation that is attached.

THIRD GENERATION DUAL-GATE ALGAN/GAN HEMT

Third generation dual-gate HEMT also had L_{G1} = 0.15 μm and L_{G2} = 0.3 μm, but an improvement in both gate lithography and material produced an f_τ of 65 GHz and a breakdown voltage of 70 V. Single gate devices with gate lengths of 0.15 μm fabricated on the same sample showed a breakdown voltage of 35 V. Third generation dual-gate HEMT achieved 12 dB small-signal gain, 3.5 W/mm saturated output power, and 45 % PAE at 8.2 GHz. All relevant plots are contained in the Power Point presentation that is attached.

CIRCUIT DESIGN

Using third generation dual-gate HEMTs, a small-signal model has been extracted from measured s-parameters, and 1-18 GHz dual-gate AlGaN/GaN power amplifier has been designed. f_τ-doubler configuration with resistive feedback has been used for the design to achieve the large bandwidth requirements. Simulation results show s21 > 10 dB with power out greater than 1.5 W across the band. Due to parasitic capacitance associated with flip-chip bonding, the decision was made to produce a monolithic microwave integrated circuit (MMIC) design on SiC. Gate lithography failure due to unstable e-beam lithography process has prevented completion of the circuit. Schematic, layout, model parameters, process, and expected performance are shown in the Power Point presentation that is attached.

CONCLUSIONS

Three generations of AlGaN/GaN dual-gate HEMTs have been produced. Third-generation AlGaN/GaN HEMT took advantage of unequal gate lengths (L_{G1} = 0.15 μm and L_{G2} = 0.3 μm) produced by e-beam lithography to simultaneously produce high f_τ (65 GHz) and large breakdown (70 V). Single gate devices with gate lengths of 0.15 μm fabricated on the same sample showed a breakdown voltage of only 35 V. Third generation dual-gate HEMT achieved 12 dB small-signal gain, 3.5 W/mm saturated output power, and 45 % PAE at 8.2 GHz. Dual-gate AlGaN/GaN HEMTs show the capability of providing the desired characteristics of a high f_τ, while still maintaining a large breakdown voltage for broadband power amplifiers. Moreover, smaller feedback capacitance and higher output impedance of dual-gate devices enable flexibility for circuit application of broadband power amplifiers.

PUBLICATIONS

[1] C.-H. Chen, K. Krishnamurthy, S. Keller, G. Parish, M. Rodwell, U. K. Mishra, and Y.-F. Wu, "AlGaN/GaN dual-gate modulation-doped field-eefect transistors,"
[2] C.-H. Chen, R. Coffie, K. Krishnamurthy, S. Keller, M. Rodwell, and U. K. Mishra,

"Dual-gate AlGaN/GaN Modulation-doped field-effect transistors with cut-off

frequencies $f_T > 60$ GHz," *IEEE Electron Device Lett.*, vol. 21, pp. 549-551, Dec. 2000.

REFERENCES

[1] Y.-F. Wu, D. Kapolnek, J. P. Ibbetson, P. Parikh, B. P. Keller and U. K. Mishra, "Very-high power density AlGaN/GaN HEMTs," *IEEE Electron Device Lett.*, vol. 48, pp. 586-590, Mar. 2001.

[2] M. Micovic, N. X. Nguyen, P. Janke, W. –S. Wong, P. Hashimoto, L.-M. McCray, C. Nguyen, "GaN/AlGaN high electron mobility transistors with f_τ of 110 GHz," *Electronic. Lett.*, vol.36, (no.4), pp. 358-359, Feb. 2000.

[3] E. O. Johnson, "Physical limitations on frequency and power parameters of transistors," *RCA Rev.*, pp. 163-177, 1965.

Dual-Gate AlGaN/GaN Modulation-Doped Field-Effect Transistors with Cut-Off Frequencies $f_T > 60$ GHz

Ching-Hui Chen, Robert Coffie, K. Krishnamurthy, Stacia Keller, Mark Rodwell, *Member, IEEE*, and Umesh K. Mishra, *Fellow, IEEE*

Abstract—We demonstrate dual-gate AlGaN/GaN modulation-doped field-effect transistors (MODFETs) with gate-lengths of 0.16 μm and 0.35 μm for the first and second gates, respectively. The dual-gate device exhibits a current-gain cut-off frequency $f_T > 60$ GHz, and can simultaneously achieve a high breakdown voltage of $>+100$ V. In comparison to single-gate devices with the same gate length 0.16 μm, dual-gate FETs can significantly increase breakdown voltages, largely increasing the maximum allowable drain bias for high power application. The continuous wave (CW) output power is in excess of 3.5 W/mm at 8.2 GHz. The corresponding large-signal gain is 12 dB and the power added efficiency is 45%. The dual-gate device with different gate lengths shows the capability of providing simultaneous high cut-off frequencies, and high breakdown voltages for broadband power amplifiers.

Index Terms—AlGaN/GaN, broadband power amplifiers, dual-gate FETs.

I. INTRODUCTION

THE 2–20 GHz PHASED array radars, now in development, require amplifiers operating over a decade bandwidth while providing tens to hundreds of watts with high power added efficiency. GaN/AlGaN-based devices exhibit large breakdown voltages (V_{br}) that enable the use of higher drain biases than typically used in other material systems to generate larger amounts of power ($P_{out} \leq V_{br}^2/8R_L$) for high power electronics. Extensive efforts toward improving microwave performance of AlGaN/GaN modulation-doped field-effect transistors MODFETs have been made in the past years [1]–[3], focusing on extending output power and cutoff frequencies, f_T. An output power density of 9.1 W/mm at 8.2 GHz has been demonstrated on SiC substrate [4] and a higher $f_T > 110$ GHz has also been achieved with a gate-length $L_g < 0.1$ μm [5].

In broadband common-source power amplifiers, the gain bandwidth product is limited to approximately f_T. Increased f_T can be obtained by reducing the gate length L_g, however, the breakdown voltage V_{br} will be significantly reduced.

In the Johnson limit [6], the product of $V_{br}f_T$ is less than $E_{max}v_{sat}/\pi$, where E_{max} and v_{sat} are the breakdown field and the electron velocity. Increased V_{br} is obtained at the expense of decreased f_T, and high power levels are obtained at the expense of reduced amplifier bandwidth.

AlGaN/GaN dual-gate devices have the potential of simultaneously realizing a high f_T and a high breakdown voltage. Moreover, smaller feedback capacitance and higher output impedance of dual-gate devices enable flexibility for circuit application of broadband power amplifiers. A dual-gate device is electrically equivalent to a common-source (CS) / common-gate (CG) cascode pair, but occupies less die area. The current gain of the dual-gate device, $h_{21}(jf) = (f_{T1}/jf)(1 + jf/f_{T2})^{-1}$, deviates from that of the CS device $h_{21}(jf) = (f_{T1}/jf)$, only for $f > f_{T2}$, where f_{T1} and f_{T2} are the current gain cutoff frequencies of the CS and CG devices and f is the signal frequency. To provide substantial current gain, f_{T1} must be several times of the signal frequency f. In contrast, to avoid significant loss (i.e., $>10\%$) in h_{21} in the CG stage, it is sufficient to have f_{T2} of 1.5 f to 2 f. The breakdown voltage is however determined by the CG device. Therefore, in a dual-gate device, it is advantageous to design the CS device with short L_g hence high f_T, and the CG device with long L_g hence lower f_T, but improved V_{br}. High bandwidth and high power are thus simultaneously obtained. In this paper, we report AlGaN/GaN dual-gate MODFETs with gate lengths of 0.16 μm and 0.35 μm for the first and second gate, respectively. A high $f_T > 60$ GHz and a high breakdown voltage of $>+100$ V can be simultaneously achieved for AlGaN/GaN MODFETs.

II. DEVICE FABRICATION

The epilayers of Al$_{0.3}$Ga$_{0.7}$N/GaN dual-gate devices were grown by metal organic chemical vapor deposition (MOCVD) on a c-plane sapphire substrate. The material structure began with a 200 Å thick GaN nucleation layer, followed by 3 μm thick insulating i–GaN as a device buffer layer. The Al$_{0.3}$Ga$_{0.7}$N contains a 30 Å unintentionally doped spacer layer, a 120 Å Si-doped charge supply layer and a 50 Å thick cap layer. Sheet electron concentration and electron Hall mobility of as-grown wafer were $\sim 1.02 \times 10^{13}$ cm^{-2} and 1400 cm^2/V-s at room temperature.

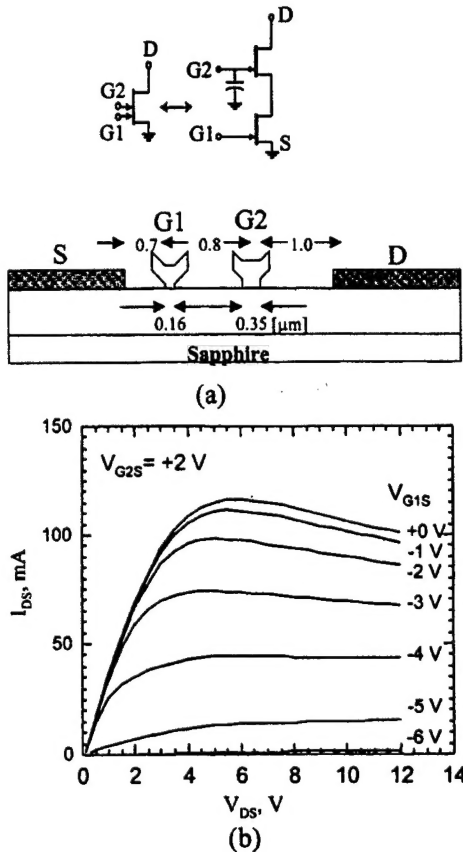Ti/Al/Ni/Au (200 Å/2000 Å/550 Å/450 Å) ohmic contacts were evaporated and then annealed at 880 °C for 30 s. Gate

(a)

(b)

Fig. 1. (a) Schematic diagram of GaN/AlGaN dual-gate FETs (b) Drain output I–V characteristics of $0.16/0.35 \times 150$ μm dual-gate MODFET's with second gate biased at $+2$ V.
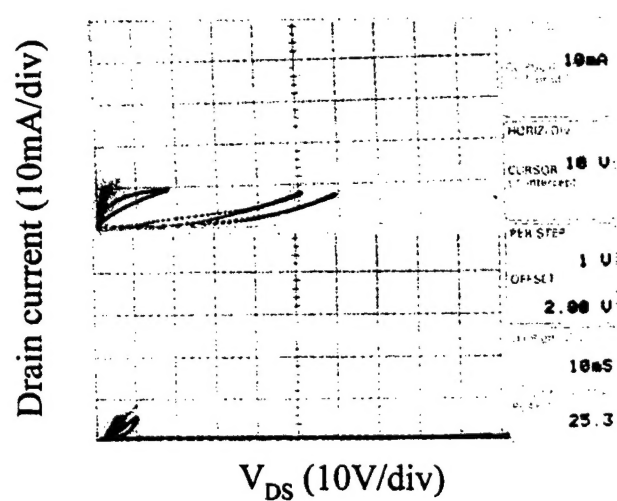

Fig. 2. Comparison of breakdown behaviors of single-gate and dual-gate GaN/AlGaN MODFETs fabricated on the same wafer. The dual-gate device increases three-terminal breakdown voltage up to $+100$ V.
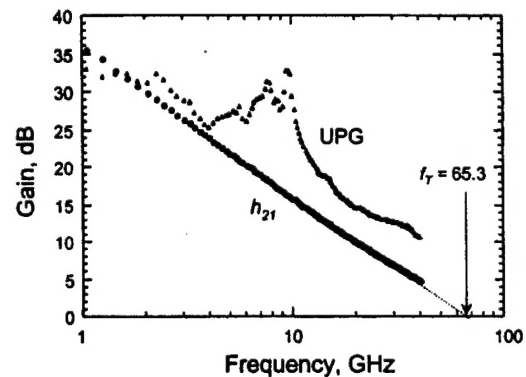

Fig. 3. Comparison of RF performance between single and dual gates devices fabricated on the same wafer: (a) S_{11}, (b) S_{22}, (c) S_{12}, and (d) S_{21}. The single-gate device was biased at $V_{DS} = +12$ V and $V_{GS} = -3$ V, and the dual-gate device was operated with bias voltages of $V_{G2S} = +2$ V, $V_{DS} = +12$ V and $V_{G1S} = -3$ V.

lithography was performed with a JEOL JBX-5DII (U) electron beam system. Both T-shaped gates with 0.16 and 0.35 μm footprints separated by 0.8 μm were produced with a PMMA/P(MMA-MAA)/PMMA tri-layer resist to reduce the resistance of submicrometer gates. Ni/Au/Ni (200 Å/3700 Å/300 Å) were then evaporated as gate metals. The gate of CG device was connected to the source of the CS device using MIM capacitors with 1600 Å SiO$_2$, providing RF grounding, and then a thick Ni/Au layer (~4500 Å) was evaporated on the top of the SiO$_2$ capacitors as the second gate pads. The final step in the process was to form a device mesa with Cl$_2$ reactive ion beam etching. The first gate was separated by 0.7 μm from the source, and the second gate was 1 μm away from the drain contact. A schematic diagram of the finished dual-gate device is shown in Fig. 1(a).

III. DEVICE CHARACTERISTICS AND DISCUSSION

The common source dc characteristics of the dual-gate device with the second gate biased at $+2$ V are shown in Fig. 1(b). The saturation current, I_{DSS}, is about 0.8 A/mm and pinch-off voltage is -6 V. The peak value of extrinsic transconductance, g_m, is about 220 mS/mm at V_{G2S} of $+2$ V. The average values of contact resistance and sheet resistance are 0.9 Ω-mm and 500 $\Omega/\square$, respectively. As seen in Fig. 2, the breakdown voltages of 0.16 μm single-gate FETs were less than $+50$ V, which is typical of such short-channel GaN/AlGaN MODFETs [8]. The

0.16/0.35 μm dual-gate FETs had larger breakdown voltages of over $+100$ V. The reason for the increased breakdown voltage is the drain voltage is supported by the longer gate, which has a higher breakdown voltage because of electric field alleviation as discussed in [7]. Since the drain voltage swing of CS device is limited to the pinch-off voltage of CG device, leakage associated with large drain voltage excursions in short-channel devices is eliminated. Therefore, the maximum allowable drain bias is increased for high frequency and high power amplifiers.

DC to 40 GHz device S-parameters were measured at a V_{DS} of $+13.5$ V, I_{DS} of 240 mA/mm, and a V_{G2S} of $+2$ V. Both CS and CG devices, we biased in the saturation region. Fig. 3 shows the h_{21} and unilateral power gain (UPG) of dual-gate devices. The dual-gate device exhibits $f_T > 65$ GHz and $f_{max} > 100$ GHz. Since the current gain of dual-gate devices follows $h_{21}(jf) = (f_{T1}/jf)(1+jf/f_{T2})^{-1}$, h_{21} of the dual-gate FETs is within roughly 10 to 20% of that of the single-gate device at the frequencies measured. Fig. 4 shows a comparison of RF performance between single-gate and dual-gate devices. Due to the presence of the second gate, the dual-gate device substantially
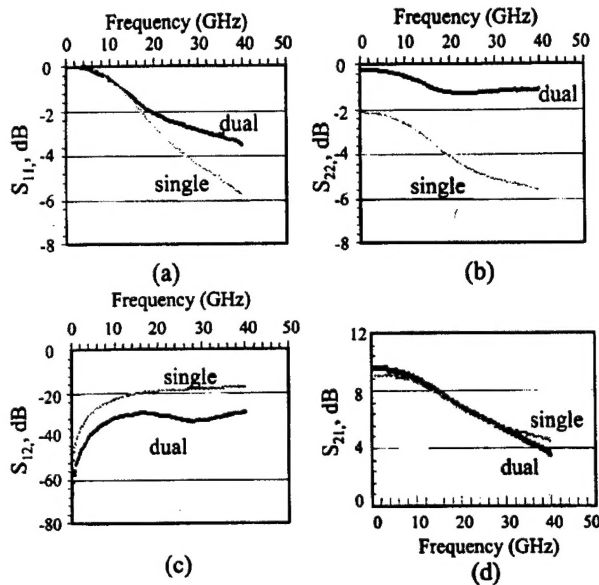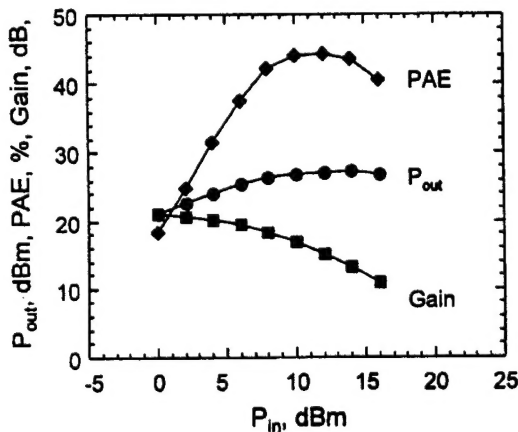
Fig. 4. Gain-frequency characteristics of dual-gate AlGaN/GaN MODFETs.

Fig. 5. Microwave power performance of dual-gate device at 8.2 GHz, with bias voltages of $V_{G2S} = +2$ V and $V_{DS} = +20$ V. The output power is greater than 3.5 W/mm, and the small signal gain, PAE, and large signal gain are 21.5 dB, 45% and 12 dB, respectively.

reduces signal feedback (S_{12}) more than 10 dB and increases output impedance (S_{22}) by 4 dB, leading to increased device power gain [9], [10]. It was noted that the maximum stable gain (MSG) and maximum available gain (MAG) of dual-gate devices were increased by 6 dB below 17 GHz, in comparison with single-gate devices. RF continuous wave (CW) power measurements were performed on uncooled devices on a sapphire

substrate at 8.2 GHz. Fig. 5 shows the power performance of dual-gate devices biased at a V_{DS} of +20 V, with the second gate bias voltage of +2 V. The drain current at peak output power was 48 mA (320 mA/mm). The output power density is higher than 3.5 W/mm. The small-signal gain, power-added efficiency (PAE), and large-signal gain are 21.5 dB, 45% and 12 dB, respectively. Unfortunately, the higher breakdown voltage afforded by this scheme could not be effectively utilized because of substrate heating effects beyond a bias of +25 V.

IV. CONCLUSIONS

In conclusion, we have demonstrated dual-gate AlGaN/GaN MODFETs with T-shaped gates of 0.16 and 0.35 μm footprints on a c-plane sapphire substrate. A CW output power in excess of 3.5 W/mm was achieved at 8.2 GHz, with power-added efficiency >45%. The dual-gate device shows a capability of providing the desired characteristics of a high f_T (>60 GHz), while still maintaining a large breakdown (>+100 V) for broadband power amplifiers.

ACKNOWLEDGMENT

REFERENCES

[1] Y.-F. Wu et al., "GaN-based FET's for microwave power amplification," IEICE Trans. Electron., vol. E82-C, pp. 1895–905, 1999.
[2] A. T. Ping et al., "DC and microwave performance of high- current AlGaN/GaN heterostructure field effect transistors grown on p-type SiC substrates," IEEE Electron Device Lett., vol. 19, pp. 54–56, 1998.
[3] S. T. Sheppard et al., "High-power microwave GaN/AlGaN HEMT's on semi-insulating silicon carbide substrate," IEEE Electron. Device Lett., vol. 20, pp. 161–163, 1999.
[4] Y. F. Wu et al., "High Al-content AlGaN/GaN HEMT's on SiC substrates with very-high power performance," in IEDM Tech. Dig., 1999, IEDM 99–925.
[5] N. X. Nguyen, "Private communication," unpublished, 1999.
[6] E. O. Johnson, "Physical limitations on frequency and power parameters of transistors," RCA Rev., pp. 163–177, 1965.
[7] T. M. Barton and P. H. Ladbrooke, "The role of the device surface in the high voltage behavior of the GaAs MESFET," Solid-State Electron., vol. 29, pp. 807–813, 1986.
[8] K. K. Chu, J. A. Smart, J. R. Shealy, and L. F. Eastman, "AlGaN-GaN piezoelectric HEMT's with submicron gates on sapphire," in Proc. Conf. Compound Semiconductor Power Transistors and State-of-the-Art Program on Compound Semiconductors (SOTAPOCS XXIX), Boston, MA, Nov. 1998.
[9] S. Asai, F. Murai, and H. Kodera, "GaAs dual-gate Schottky-barrier FET's for microwave frequencies," IEEE Trans. Electron Devices, vol. ED-22, pp. 897–904, Oct. 1975.
[10] Y. K. Chen, G. W. Wang, D. C. Radulescu, and L. F. Eastman, "Comparison of microwave performance between single-gate and dual-gate MODFETs," IEEE Electron. Device Lett., vol. 9, pp. 59–61, Feb. 1988.

regions while ignoring all buildings which block the lit regions, we define that the two VSs look at each other. In this procedure, the transmitter and the receiver are considered as VSs, and the lower bounds of all lit regions are then ignored. From the pairs of VSs, rays from the transmitter to the receiver are found by backward ray tracing in the plan view. The rays over buildings in the plan view account for forward rooftop diffractions. Since two sets of VSs are constructed, there may be duplicated rays, and so they must be removed.
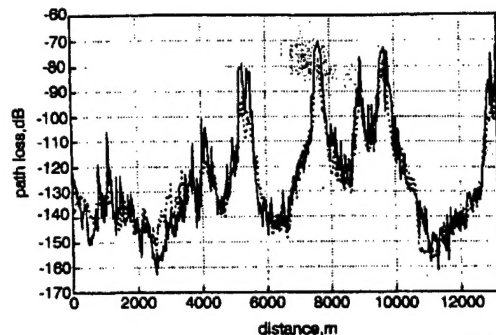
Fig. 4 *Comparison of predictions with measurements*

——— predictions
– – – – measurements

In the second step, for each ray in the plan view, the entire series of horizontal building edges lying between the transmitter and the receiver is available as the unfolded vertical profile of buildings. Using the vertical profile, the heights of the scattering points around buildings, as well as forward and backward rooftop diffraction points can be determined in a similar manner to that in [2], with the approximation that the rays diffracted at a horizontal edge are taken to lie in the plane of the vertical profile. This approximation introduces a small prediction error.

To determine the diffraction loss due to propagation over buildings, we first find significant edges which form the shortest path from the transmitter to the receiver and apply the UTD diffraction coefficients to those edges in a cascade. When applying the UTD, the edges in the transition region of a previous edge are excluded, and the accounted edges as well as the transmitter and the receiver are set to the 'UTD edge's'. Between each pair of 'UTD edge's' there can be additional edges that may interfere with the propagation field. Among those edges, the most significant edges up to 10 are accounted for by the method proposed by Whitteker [3] in the calculation of the additional loss. From one vertical profile, multiple rays which may undergo back diffractions from horizontal edges or ground reflections can be found, and they must be considered individually. Our method allows for a single back diffraction from a horizontal edge anywhere along the ray path. The Fresnel reflection coefficients and the UTD diffraction coefficients are then applied for the scatterings around the buildings.

For computational efficiency, we constructed two VSTs in the restricted areas around a transmitter and a receiver within radii R_T and R_R as shown in Fig. 2. This restriction causes a slight prediction error in most cases, and the radius must be larger as the source height is increased.

Results and conclusion: To check the accuracy of the proposed ray tracing method, prediction results are compared with measurements in Munich which have been supplied by the German GSM operator Mannesmann Mobilfunk GmbH. Fig. 3 shows the building layouts in the city as well as the transmitter location and measurement route. The measurements were carried out at 947MHz with the transmitter and receiver heights 13 and 1.5m above the ground, respectively. To predict the signal path loss, scatterings up to 3rd order including one diffraction were allowed in the areas within $R_T = 500m$ and $R_R = 200m$, respectively. The sector averaged received power was calculated by summing the individual powers of the contributing rays [2]. The values of relative permittivity and conductivity were set at 4.44, 0.01S/m for buildings and 15, 7S/m for the ground.

Fig. 3 shows some dominant rays from the transmitter to one receiver in the measurement route. The detailed comparisons in the route are shown in Fig. 4. The average and standard deviation of the prediction error are 1.83 and 7.84dB, and so the predictions of the proposed method are in good agreement with the measurements.

Hae-Won Son and Noh-Hoon Myung (*Department of Electrical Engineering, Korea Advanced Institute of Science and Technology, (KAIST), 373-1, Kusong-dong, Yusong-gu, Taejon, Korea*)

E-mail: hwson@cais.kaist.ac.kr

References

1   RIZK, K., WAGEN, J.F., and GARDIOL, F.: 'Two-dimensional ray tracing modeling for propagation prediction in microcellular environments', *IEEE Trans.*, 1997, VT-46, (2), pp. 508–518
2   LIANG, G., and BERTONI, H.L.: 'A new approach to 3-D ray tracing for propagation prediction in cities', *IEEE Trans.*, 1998, AP-46, (6), pp. 853–863
3   WHITTEKER, J.H.: 'Near-field ray calculation for multiple knife-edge diffraction', *Radio Sci.*, 1984, 19, (4), pp. 975–986

AlGaN/GaN dual-gate modulation-doped field-effect transistors

C.-H. Chen, K. Krishnamurthy, S. Keller, G. Parish, M. Rodwell, U.K. Mishra and Y.-F. Wu

The first results concerning dual-gate AlGaN/GaN MODFETs are presented. The devices have 0.65μm gate lengths and were grown by metal organic chemical vapour deposition (MOCVD) on a sapphire substrate. The continuous wave (CW) output power is in excess of 2.5W/mm at 4GHz. The corresponding large-signal gain is 11.5dB and the power added efficiency is 30.6%. Dual-gate devices with different gate lengths can provide simultaneous high breakdown voltage and high current-gain cutoff frequency for the broadband power amplifiers.

2–20GHz phased array radars, now in development, require amplifiers operating over a decade bandwidth while providing tens to hundreds of Watts with high power added efficiency. GaN-based modulation-doped field-effect transistors (MODFETs) are attractive in high power applications due to a large breakdown voltage V_{bv} ($P_{out} \leq V_{bv}^2/8R_L$) [1 – 3]. 6W/mm power density at 10GHz has been demonstrated for devices on SiC substrate [3]. $f_T > 60GHz$ has been achieved with a gate length $L_g < 0.15μm$ [4]. In broadband commonsource power amplifiers, the gain bandwidth product is limited to $\sim f_T$. Decreasing L_g increases f_T, with the product $V_{bv}f_T < E_{max} v_{sat}/\pi$, where E_{max} and v_{sat} represent the breakdown field and electron velocity [5]. Increased V_{bv} is obtained at the expense of decreased f_T, and high power levels are obtained at the expense of reduced amplifier bandwidth.

A dual-gate device is electrically equivalent to a common-source (CS)/common-gate (CG) cascode pair [6], but occupies less die area. The current gain of the dual-gate device, $h_{21}(jf) = (f_{T1}/jf)(1 + jf/f_{T2})^{-1}$, deviates from that of the CS device $h_{21}(jf) = (f_{T1}/jf)$, only for $f > f_{T2}$, where f_{T1} and f_{T2} are the current gain cutoff frequencies of the CS and CG devices. To provide substantial current gain, f_{T1} must be several times the signal frequency f. In contrast, to avoid significant loss in h_{21} in the CG stage, it is sufficient to have an f_{T2} of 1.5–2f. The breakdown voltage is however determined by the CG device. Therefore, in a dual-gate device, it is advantageous to design the CS device with short L_g, hence high f_{T1}, and the CG device with long L_g, hence lower f_{T2}, but improved V_{bv}. High bandwidth and high power are thus simultaneously obtained.

As a first demonstration, we fabricated dual-gate $Al_{0.25}Ga_{0.75}N$/GaN MODFETs with equal gate length (0.65μm) for CS and CG devices. Details of the epitaxial structure and fabrication process can be found in [1]. The sheet electron concentration and electron Hall mobility of as-grown modulation doped structures were ~1.72

$\times 10^{13} \text{cm}^{-2}$ and $\sim 950 \text{cm}^2/\text{V s}$ at room temperature. The gate of the CG device was connected to the source using MIM capacitors with 1000Å SiO_2 providing RF grounding. The first gate was separated by 0.7μm from the source and by 1.5μm from the second gate.
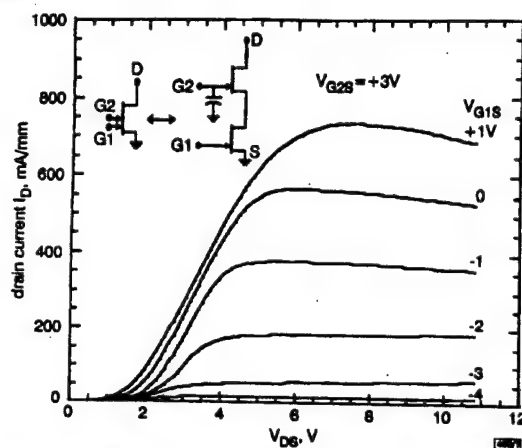

Fig. 1 *Drain output I-V characteristics of 0.65 × 150μm dual-gate AlGaN/GaN MODFETs, with second gate biased at +3V*

Maximum current > 700mA/mm

Fig. 1 shows the common source DC characteristics with the second gate biased at +3V. The pinch-off voltage is ~-4V and the gate-drain breakdown voltage is > 60V. Varying V_{G1S} varies V_{D1S}, hence the saturation current I_{DSS} and extrinsic transconductance g_m increase as V_{G1S} increases. The maximum transconductance g_m is ~205mS/mm.
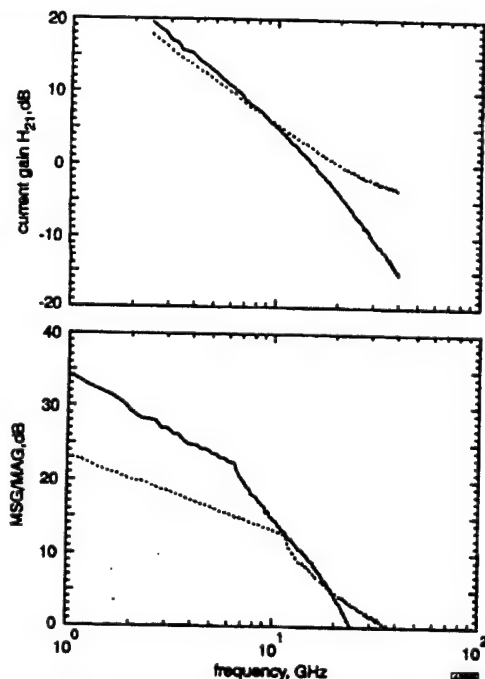
Fig. 2 *Gain-frequency characteristics of single-gate and dual-gate AlGaN/GaN MODFETs*

Drain biased conditions: +7V × 220mA/mm for single-gate device; +12V × 130mA/mm for dual-gate device
——— dual gate
– – – – single gate

DC to 40GHz device S-parameters were measured at a V_{DS} of +12V, and gate bias voltages of V_{G1S} = −2V and V_{G2S} = +3V, respectively. Both CS and CG FETs operate in the saturation

region under this biasing condition. Fig. 2 shows a comparison of the h_{21} for single-gate and dual-gate MODFETs on the same wafer. The single-gate device exhibits $f_T \simeq 20.3$GHz and $f_{max} \simeq 38.5$GHz. The dual-gate device shows $h_{21}(jf) = (f_{T1}/jf)(1 + jf/f_{T2})^{-1}$, with f_{T1} = 22.2GHz and f_{T2} = 14.5GHz, and $f_{max} \simeq 24.2$GHz. Owing to the reduced feedback signal (S_{12}) and increased output impedance (S_{22}) [6], the MSG/MAG of the dual-gate device is increased by 10dB for frequencies below 7GHz. Continuous wave (CW) microwave power measurements at 4GHz were performed on uncooled devices on sapphire substrate. The dual-gate device was biased at a source-drain voltage of +27.5V, and the second gate bias voltage V_{G2S} was +5.5V. The drain current at peak output power was 40mA (266mA/mm). The peak output power, as shown in Fig. 3, is 25.7dBm, corresponding to a 2.5W/mm power density. The small-signal linear gain, power added efficiency (PAE), and large-single gain are 17.6dB, 30.6%, and 11.5dB, respectively.
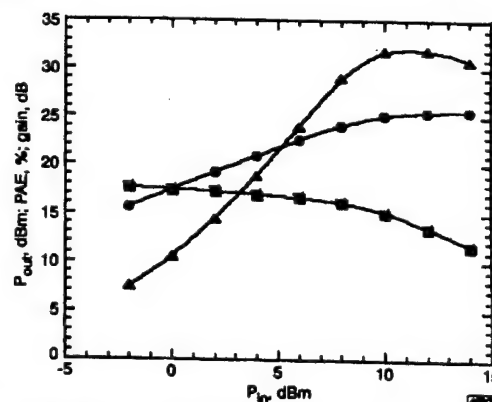
Fig. 3 *Microwave power performance of dual-gate device at 4 GHz*

Source-drain voltage was +27.5V, and second gate was biased at voltage V_{G2S} of +5.5V; small-signal linear gain is ~17.6dB, peak output power density is > 2.5W/mm, corresponding large-signal gain, and power added efficiency (PAE) are 11.5dB and 30.6%
▲ PAE
● P_{out}
■ gain

We have demonstrated the first dual-gate $Al_{0.25}Ga_{0.75}N/GaN$ MODFETs. A CW output power in excess of 2.5W/mm was achieved at 4GHz, with power added efficiency > 30%. In the future, to obtain the desired characteristics of a high f_T (> 50GHz) while maintaining a large output power for broadband power amplifiers, the common-source device will be designed for a high f_T ($L_g \leq 0.15$μm) hence low breakdown V_{br}, and the common-gate device can be designed for high V_{br} and consequently low f_T.

C.-H. Chen, K. Krishnamurthy, S. Keller, G. Parish, M. Rodwell and U.K. Mishra (*Department of Electrical and Computer Engineering, University of California, Santa Barabara, CA 93106, USA*)

Y.-F. Wu (*WiTech, 107 S. La Patera Lane, Goleta, CA 93117, USA*)

References

1   WU, Y.-F., KELLER, B.P., KELLER, S., NGUYEN, N.X., LE, M., NGUYEN, C., JENKINS, T.J., KEHIAS, L.T., DENBAARS, S.P., and MISHRA, U.K.: 'Short channel AlGaN/GaN MODFETs with 50-GHz f_T and 1.7W/mm output power at 10GHz', *IEEE Electron Device Lett.*, 1997, 18, (9), pp. 438–440

2   PING, A.T., CHEN, Q., YANG, J.W., KHAN, M.A., and ADESIDA, I.: 'DC and microwave performance of high-current AlOaNlOaN heterostructure field effect transistors grown on p-type SiC substrates', *IEEE Electron Device Lett.*, 1998, 19, (2), pp. 54–56

3 SHEPPARD, S.T., DOVERSPIKE, K., PRIBBLE, W.L., ALLEN, S.T., and PALMOUR, J.W.: 'High power microwave GaN/AlGaN HEMTs on silicon carbide'. 56th Device Research Conf. Dig., 1998
4 CHU, K.K., CHUMBES, E.M., GREEN, B.M., SHEALY, J.R., and EASTMAN, L.F.: Unpublished, 1998
5 JOHNSON, E.O.: 'Physical limitations on frequency and power parameters of transistors', RCA Rev., 1965, pp. 163–177
6 ASAI, S., MURAI, F., and KODERA, H.: 'GaAs dual-gate Schottky-barrier FET's for microwave frequencies', IEEE Trans., 1975, ED-22, (10), pp. 897–904

Mid-infrared intersubband electroluminescence in InAs/AlSb cascade structures

K. Ohtani and H. Ohno

Mid-infrared intersubband electroluminescence is reported in InAs single quantum wells embedded in InAs/AlSb quantum cascade structures. The observed emission energy is in good agreement with calculations based on the multiband k·p theory. The dominant polarisation of the emitted light is perpendicular to the quantum well layers.

Quantum cascade lasers (QCL) are high performance mid-infrared light sources based on intersubband optical transitions, first demonstrated using GaInAs/AlInAs quantum well (QW) structures [1, 2]. The wavelength range covered by GaInAs/AlInAs QCLS includes the atmospheric windows (3–5 and 8–13μm) important for gas sensing and environment monitoring applications. Recently, high power continuous-wave (CW) operation (5 and 8μm, 200mW/facet) has been achieved at 80K [3, 4].

Sb-based InAs/AlSb QCLs have a number of advantages over GaInAs/AlIAs QCLs. The InAs/AlSb heterostructure has a highly tunable intersubband transition energy due to the larger conduction band offset (~1.35eV) compared to that of the GaInAs/AlInAs systems (~ 0.5eV). Also, a recent theoretical appraisal of Sb-based intersubband lasers (5μm) [5, 6] showed that the threshold current density can be as low as 750A/cm² at 300K, almost a factor of four lower than the theoretical prediction for the 5μm GaInAs/AlInAs QCLs [6]. This is due to the small electron effective mass in the InAs QW, which reduces the optical phonon scattering rate believed to account for the high threshold current density in GaInAs/AlInAs QCLs, and at the same time increases the dipole matrix elements of the intersubband transition. Although intersubband electroluminescence in InAs QWs utilising interband tunnelling between InAs/GaSb has been realised recently [7], electroluminescence from InAs/AlSb structures has not yet been achieved. In this Letter, we report the first observation of mid-infrared intersubband electroluminescence in InAs single QWs embedded in InAs/AlSb quantum cascade structures.

The samples were grown by a solid source molecular beam epitaxy system equipped with a compound As cell and a cracking Sb cell on undoped InAs(100) substrates. After the growth of 700nm Si-doped (3×10^{17}cm⁻³) n-type InAs as a bottom contact layer, 10 periods of injector and active layer structures were grown. The injector structure consisted of digitally graded InAs/AlSb superlattices in which the InAs layers were Si-doped to $n = 2 \times 10^{17}$cm⁻³. The active layer consisted of an InAs/AlSb single QW which comprised a 10ML AlSb barrier, a 30ML InAs quantum well, and a 5ML AlSb barrier. An alternate structure which had a thinner InAs well (26ML) was also grown. After growth of the injector/active layer structures, 200 nm Si-doped (3×10^{17}cm⁻³) InAs was grown as a top contact layer. All layers were grown at 420°C. During growth of injector and active layers, the InAs growth rate was reduced to 0.2ML/s and the As pressure was kept at a minimum to yield the group-V stability condition in order to prevent As incorporation into Sb-based layers. The AlSb layers displayed 1×3 RHEED patterns, and the InAs layers displayed 2×1 RHEED patterns with a V/III beam equivalence pressure ratio of 5.5 for InAs and AlSb growth.

The grown sample was then processed into a 200μm × 200μm mesa by wet-etching and photolithography. Non-alloyed Cr/Au ohmic contacts were deposited on both top and bottom contact

layers. The sample edge was then polished to a 45° wedge for light emission and mounted onto a copper cold finger of a cryostat for cooling down to ~ 77K. The electroluminescence measurement was performed with a rapid scan FT-IR spectrometer (Bio-Rad FTS-60A) using a lock-in detection technique with a resolution of 4cm⁻¹ [8]. A liquid-nitrogen cooled HgCdTe detector was used; a polariser was inserted in the optical path to verify the polarisation of the emission. Current pulses at 15kHz with a duty cycle of 50% were used for the electroluminescence measurements. Under a forward bias, electrons are injected from an injection region into the first excited state (E_2) of the InAs QW. The electrons at E_2 undergo intersubband transitions (radiative and nonradiative) and relax to the ground state (E_1) of the InAs QW. The relaxed electrons then tunnel to the collector through a thin AlSb barrier; the collector acts as an injector for the next QW. From the multiband k.p theory [9], the energy separation between E_1 and E_2 of the 30ML InAs quantum well sample is 228meV and that of the 26ML sample is 267meV.
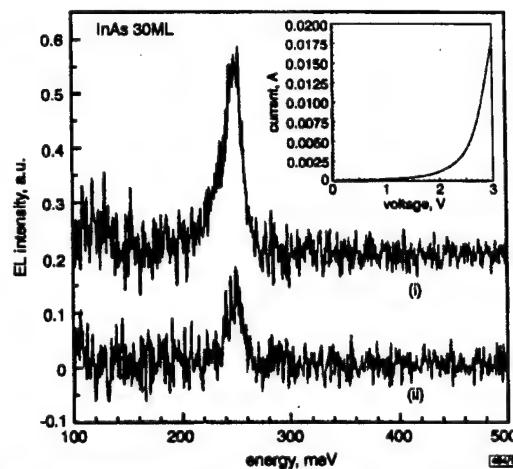

Fig. 1 *Electroluminescence spectra at ~77K for different injection currents*

(i) 80 mA
(ii) 50 mA
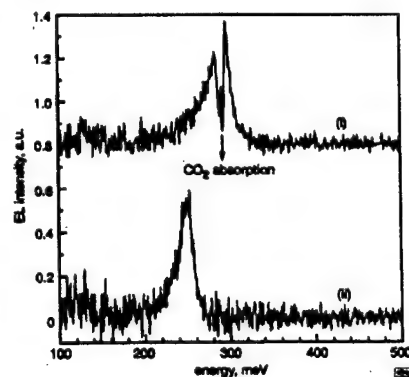Inset: current-voltage characteristics at ~77K of intersubband cascade structure. Mesa area is 200μm × 200μm

Fig. 2 *Electroluminescence spectra of intersubband cascade structures at ~77K for 80mA injection current density*

(i) 26 ML
(ii) 30 ML
Mesa area is the same for both samples

A typical current-voltage characteristic at ~77K is shown in the inset of Fig. 1. The injector blocks the current up to a bias of ~2.5V, after which the alignment of the injectors leads to current flow. Fig. 1 shows the electroluminescence spectra at ~77K under two different current bias conditions. An emission peak was observed at 247meV, corresponding to a wavelength of 5μm with full width at half maximum of ~18meV. The emission energy is in

Device Approaches

Why Dual-gate / Casode HEMTs?

-> "slow-fast" cascode

FET 2 *slow, high V_{br}*

FET 1 *fast, low V_{br}*

D

G_2

G_1

S

D

G_2 G_1

S
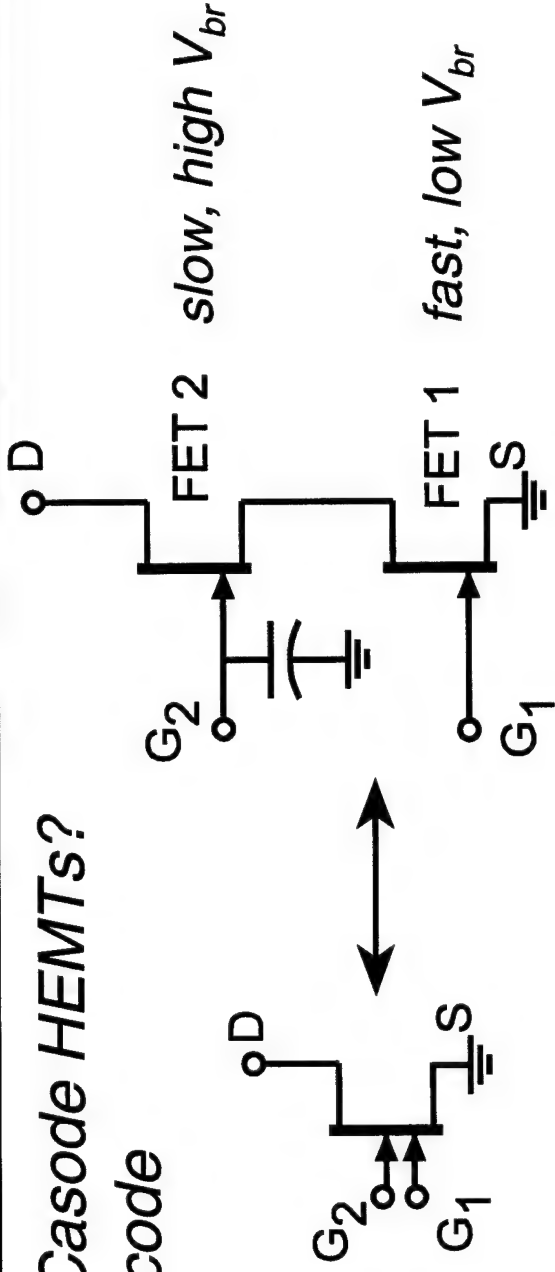
FET 1

- Limits amplifier bandwidth $\sim f_{\tau 1}$/gain
- Small $V_{DS1} \sim 10$ V

FET 2

- Introduces a pole at $f_{\tau 2}$
- Large $V_{DS2} \sim 100$V

- FET 1 needs high $f_{\tau 1}$ (> 50 GHz, $L_{G1} < 0.15 \, \mu m$), low breakdown
- FET 2 needs high breakdown, lower $f_{\tau 2}$ ($L_{G2} \sim 0.5 \, \mu m$),

High breakdown and high f_τ attained simultaneously

UCSB

Accomplishments:
First Dual-gate GaN HEMTs

First-Generation Device:

$L_{G1} = L_{G2} = 0.65$ microns
20 GHz current-gain cutoff frequency
60 V breakdown
2.5 W/mm, 35% PAE,
11 dB gain at 4 GHz

Suboptimal device: need $L_{G1} << L_{G2}$
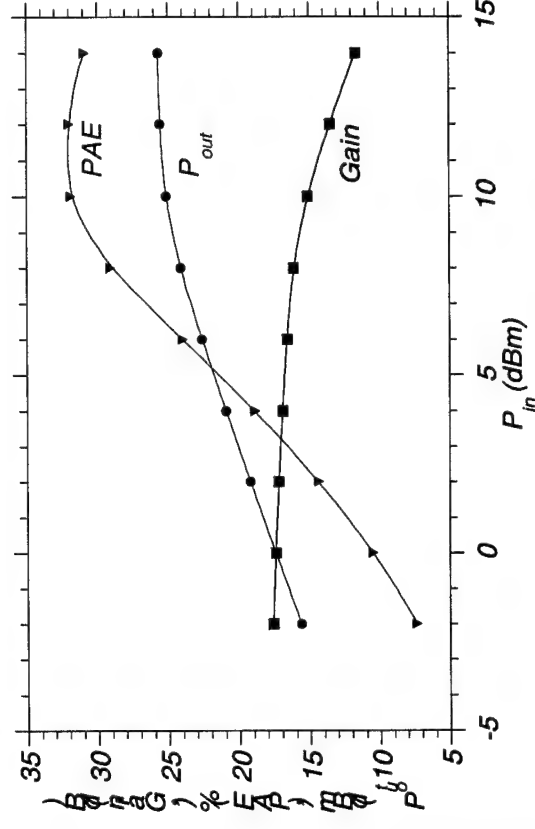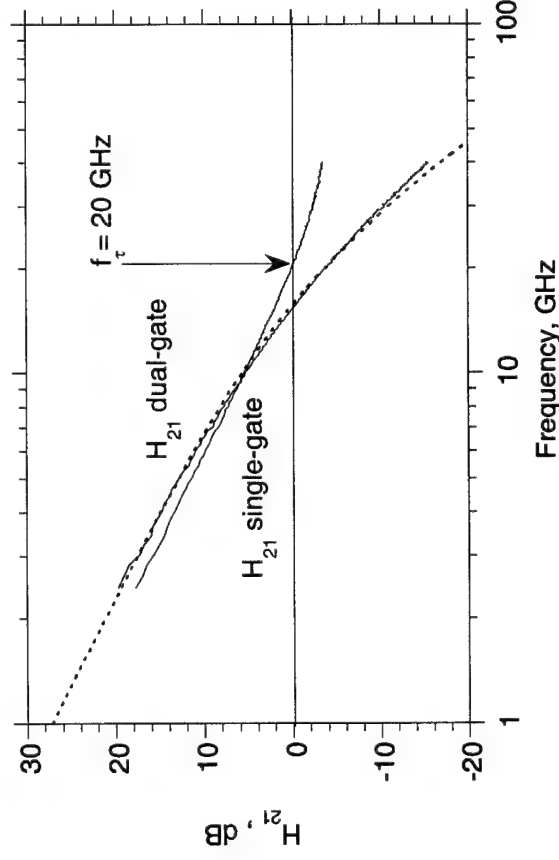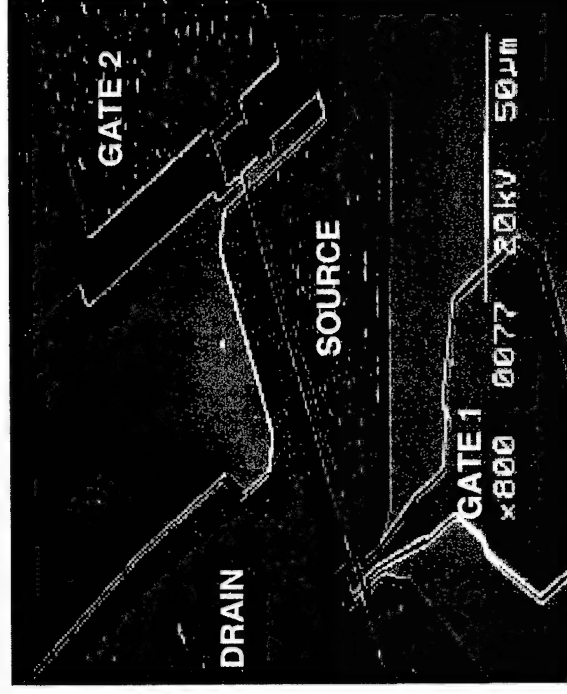
Accomplishments: UCSB
Deep submicron dual-gate GaN HEMTs

mobility ~ 1100 cm^2/V-s
charge n_s ~ 1.1×10^{13} cm^2

$L_{G1} = 0.15\ \mu m$
$L_{G2} = 0.3\ \mu m$

S G1 G2 D
$0.7\ \mu m$ $0.9\ \mu m$ $1.0\ \mu m$
AlGaN
GaN
Sapphire substrate

G1 G2 ~ 0.16 μm

Second-Generation Device:

L_{G1} = 0.15 μm; small for high f_τ ;
L_{G2} =0.3 μm; large for high breakdown

52 GHz current-gain cutoff frequency

8 dB current gain at 20 GHz

> 100 V breakdown

Drain current (10mA/div)

V_{DS} (10V/div)

Accomplishments:
Deep submicron dual-gate GaN HEMTs — UCSB

mobility ~ 1100 cm²/V-s
charge n_s ~ 1.1 x 10^{13} cm⁻²

S G1 G2 D

0.7 μm | 0.9 μm | 1.0 μm

AlGaN

GaN

Sapphire substrate

$L_{G1} = 0.15\ \mu m$
$L_{G2} = 0.3\ \mu m$

Second-Generation Device:

L_{G1} = 0.15 μm; small for high f_τ ;
L_{G2} =0.3 μm; large for high breakdown

52 GHz current-gain cutoff frequency

8 dB current gain at 20 GHz

>100 V breakdown

high small-signal power gain

dual gate

single gate

MSG/MAG, dB

40 — 30 — 20 — 10 — 0

Frequency, GHz   1   10   100

52 GHz f_τ

single gate

dual gate

68.2
52.3

H_{21}, dB

40 — 30 — 20 — 10 — 0

Frequency, GHz   1   10   100

Accomplishments:
Deep submicron dual-gate GaN HEMTs

mobility ~ 1100 cm^2/ V-s
charge n_s ~ 1.1 x 10^{13} cm^{-2}

L_{G1} = 0.15 μm
L_{G2} = 0.3 μm

S   G1   G2   D

| 0.7 μm | 0.9 μm | 1.0 μm |

AlGaN

GaN

Sapphire substrate

G2

G1

~ 0.16 μm

Third-Generation Device:

L_{G1} = 0.15 μm; small for high f_τ ;
L_{G2} = 0.3 μm; large for high breakdown

65 GHz current-gain cutoff frequency
3.5 W/mm, 45 % PAE,
12 dB gain at 8.2 GHz
70 V breakdown

dual-gate

Drain current (500 uA/div)

V_{DS} (10V/div)

UCSB

Accomplishments:
Deep submicron dual-gate GaN HEMTs

mobility ~ 1100 cm^2/V-s
charge n_s ~ 1.1 x 10^{13} cm^{-2}

$L_{G1} = 0.15$ μm
$L_{G2} = 0.3$ μm

S   G1   G2   D

0.7 μm 0.9 μm 1.0 μm

AlGaN
GaN
Sapphire substrate

Third-Generation Device:
$L_{G1} = 0.15$ μm; small for high f_τ ;
$L_{G2} = 0.3$ μm; large for high breakdown

65 GHz current-gain cutoff frequency
3.5 W/mm, 45 % PAE,
12 dB gain at 8.2 GHz
70 V breakdown

PAE
P_{out}
Gain
f = 8.2 GHz
P_{in}, dBm
P_{out}, dBm, PAE, %, Gain, dB

65 GHz f_τ
f_T = 65.3
h_{21}
H_{21}, dB
Frequency, GHz

Circuit Options

UCSB

Lumped circuits: limited by f_{max} and f_τ

Distributed circuits: limited only by f_{max}

f_τ multipliers: also limited only by f_{max}

f_τ Multiplier Principle of Operation   UCSB

Simple Stage

$$\frac{I_{out}}{I_{in}} = \frac{1}{j}\left(\frac{f_\tau}{f}\right)$$

f_t Doubler

$$\frac{I_{out}}{I_{in}} = \frac{1}{j}\left(2\cdot\frac{f_\tau}{f}\right)$$
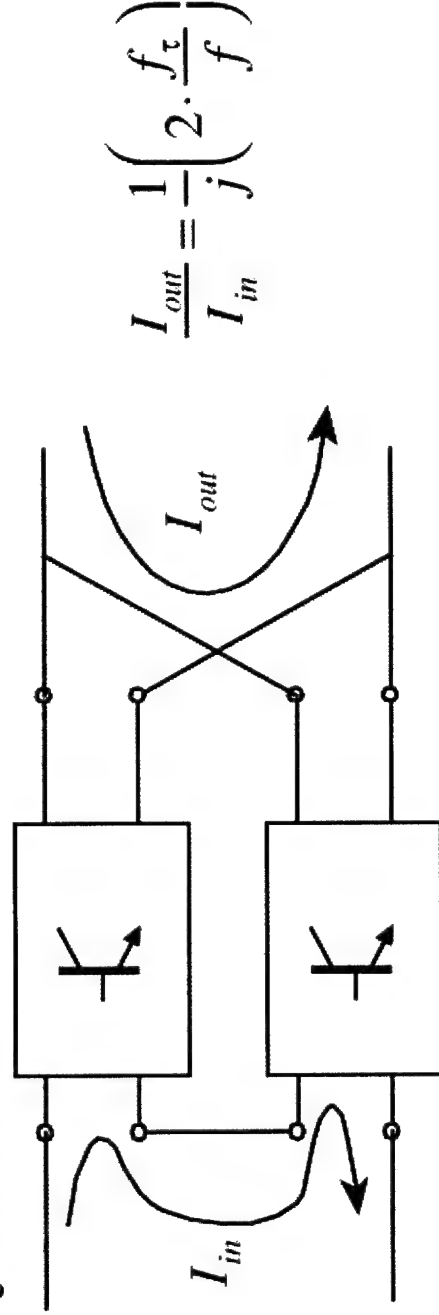
Inputs connected in series, outputs connected in parallel output currents add

current gain is twice that of single stage, f_τ is doubled
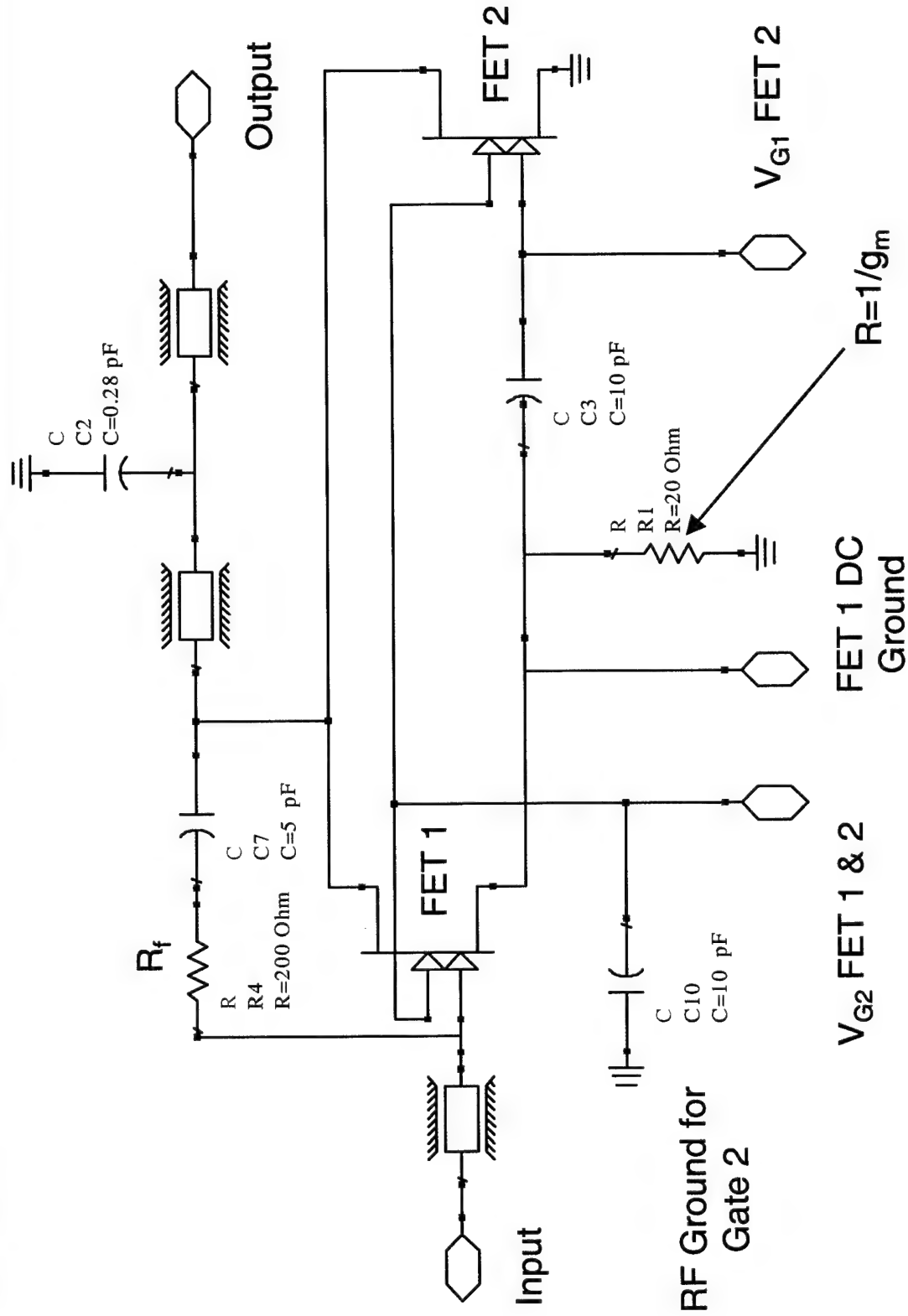
Circuit Simulations

UCSB

Intrinsic Device Parameters:

$g_m = 150$ mS/mm $C_{gs} = 430$ fF/mm

$R_i = 5 \ \Omega$mm $\quad C_{gd} = 22$ fF/mm

$R_{ds} = 60 \ \Omega$mm $\quad f_\tau = 55$ GHz

Measured from third-generation devices

MMIC Chip:

SiC Substrate

Co-planar Wave Guide Design

f_τ doubler configuration with resistive feedback

Total Gate Periphery = 1.2 mm

Die Dimensions: W = 2.65 mm L = 2.10 mm
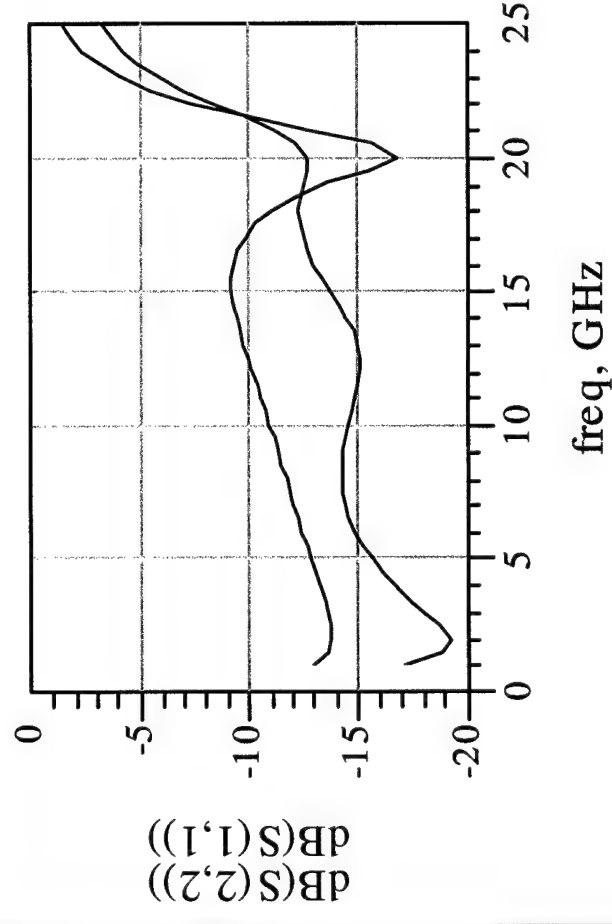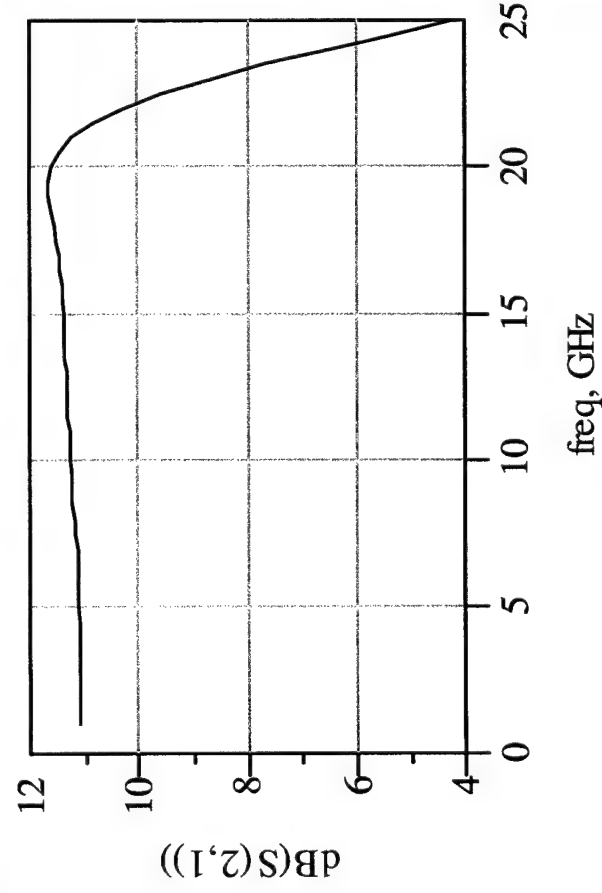
UCSB

Circuit Simulations

Large Signal Simulations:

P1dB > 1 W from 1 – 20 GHz

Peak PAE = 20 %

Peak Pout = 3 W

Large Signal Simulations:

Soft saturation of GaN HEMT not taken into account in simulation

Simulated Circuit Characteristics

Typical Measured Characteristics
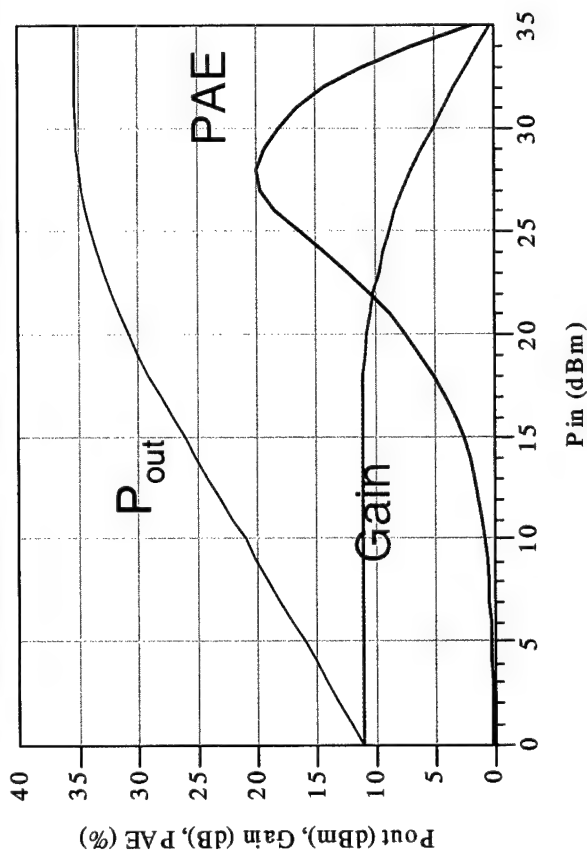
Circuit Simulations

Darlington Configuration without $1/g_m$ resistor in source path of FET 1

Instability due to negative input resistance
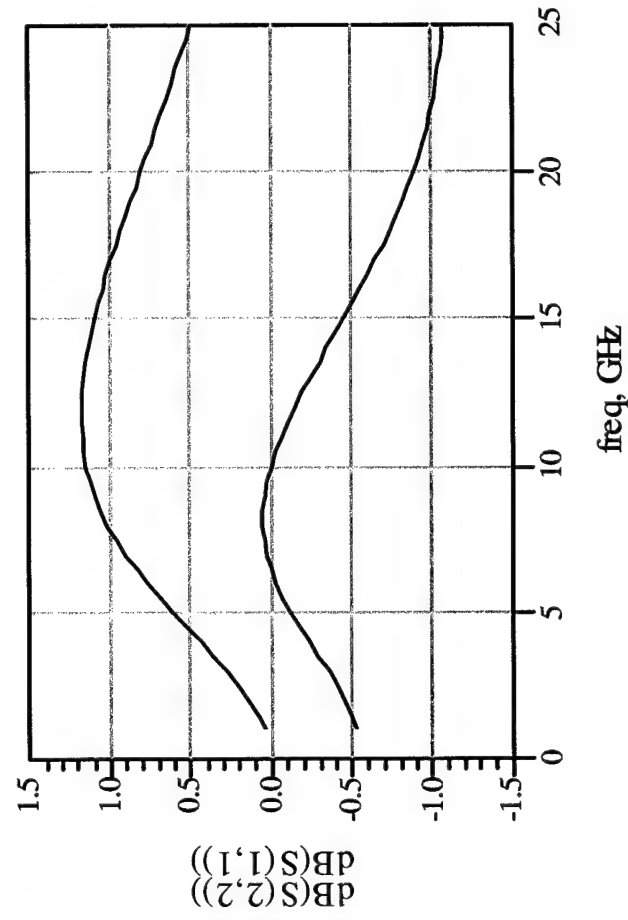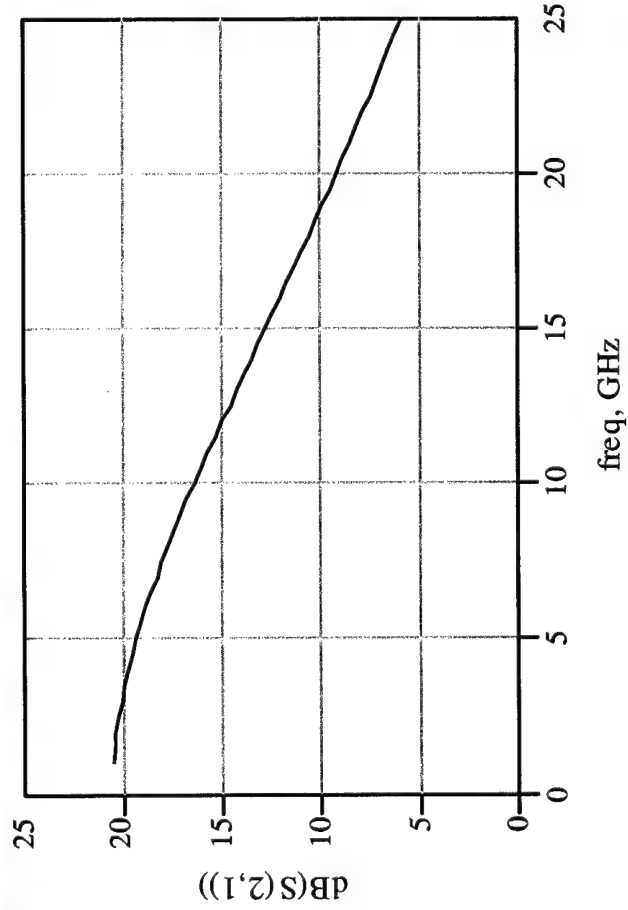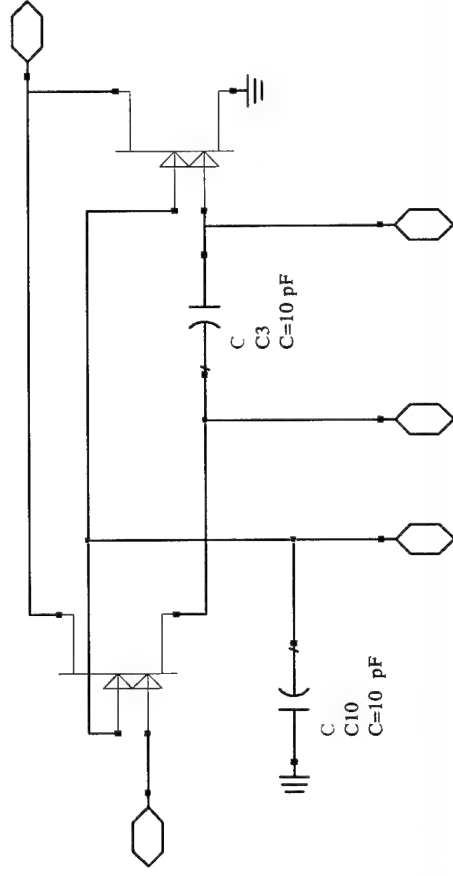
Circuit Simulations

Darlington Configuration with 1/g_m resistor in source path of FET 1

1/g_m resistance removes negative input impedance

1/g_m value chosen so FETs provide equal currents at all frequencies

Immediate improvement in S11 observed

C
C3
C=10 pF

R
R1
R=20 Ohm

C
C10
C=10 pF

dB(S(2,2))
dB(S(1,1))

freq, GHz

0.2 0.0 -0.2 -0.4 -0.6 -0.8 -1.0 -1.2

0 5 10 15 20 25

dB(S(2,1))

freq, GHz

25 20 15 10 5 0

0 5 10 15 20 25
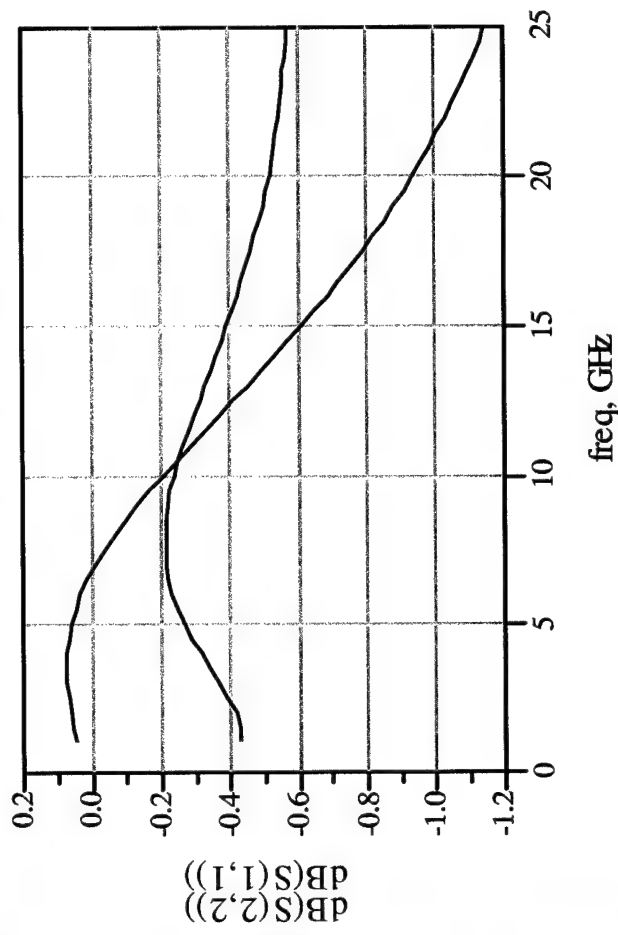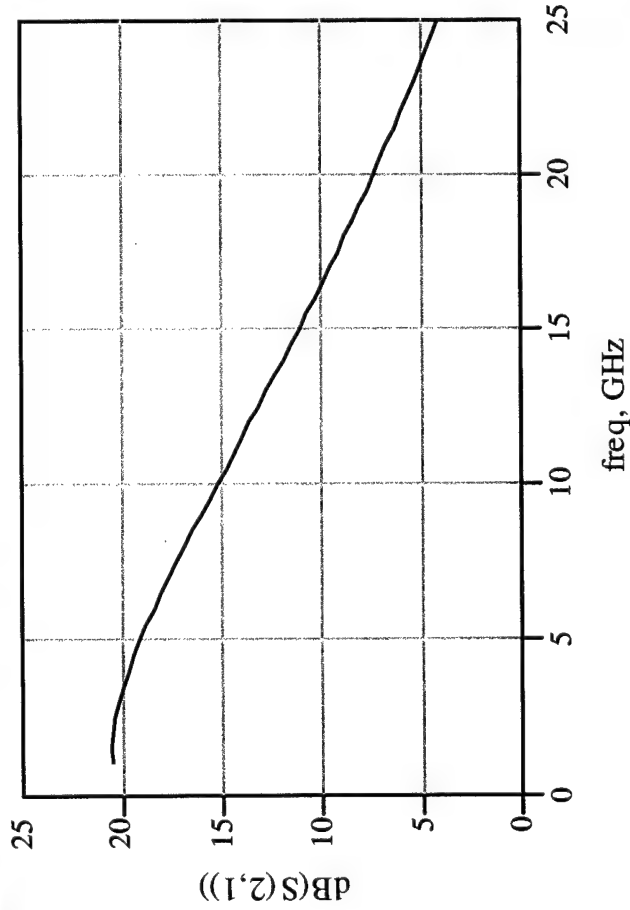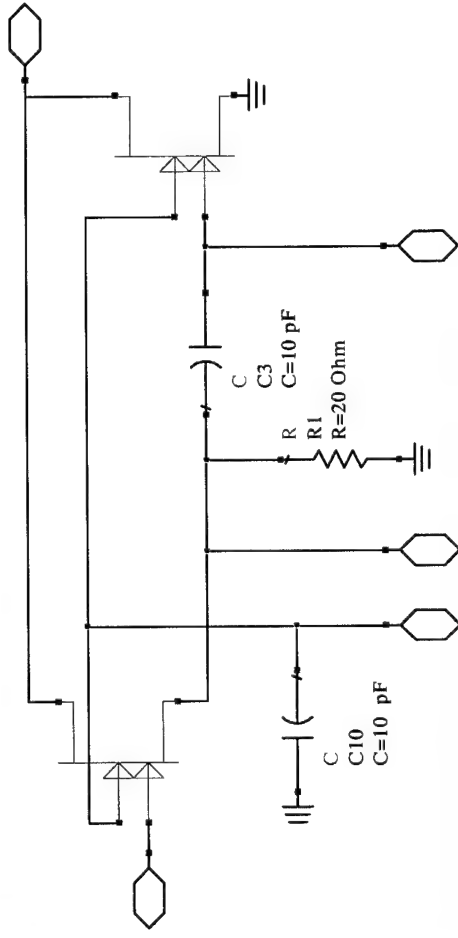
UCSB

Circuit Simulations

Resistive feedback added to circuit

$R_f = Z_o(1-A_v)$ provides input and output matching at lower frequencies (< 10 GHz)

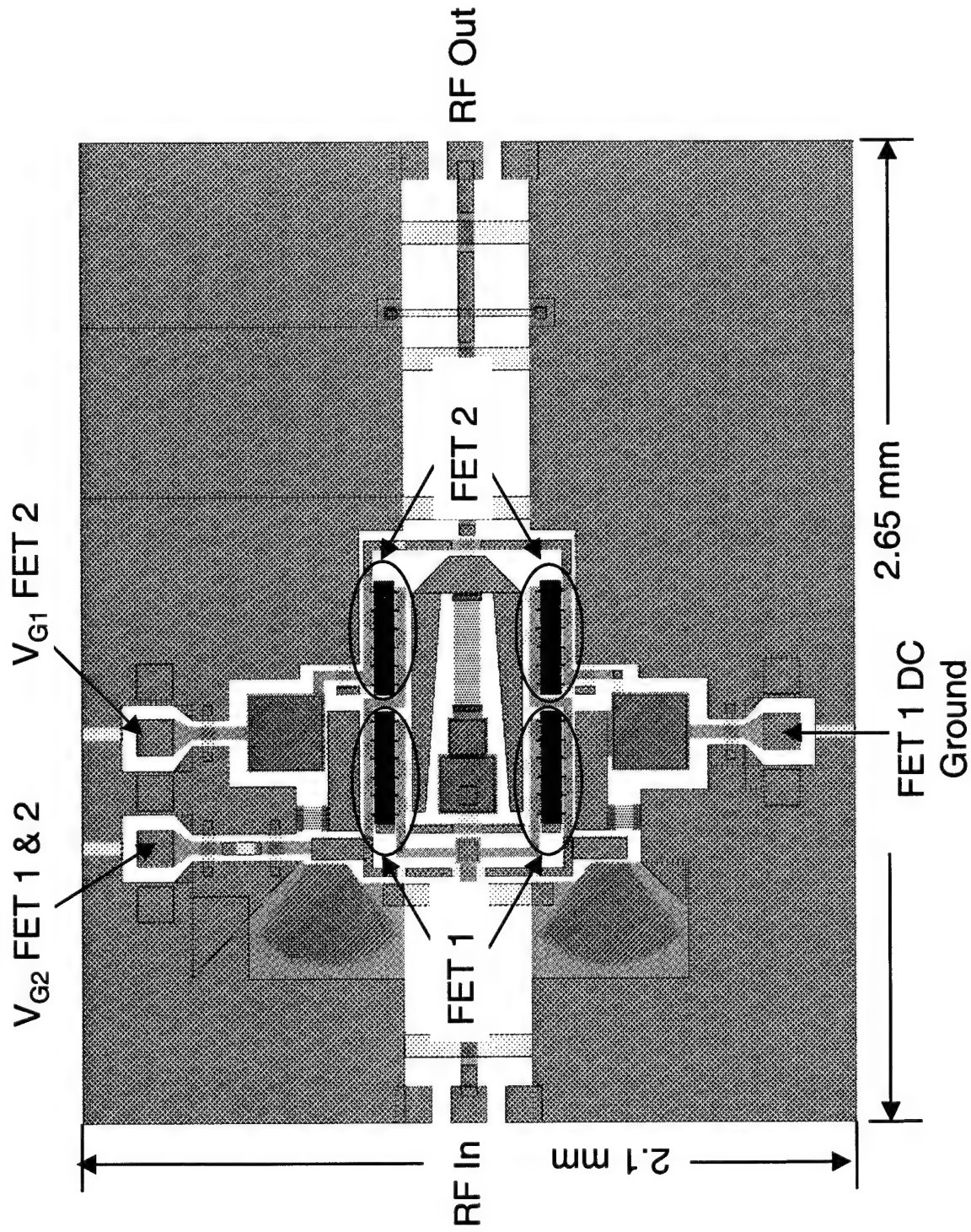Flat gain response is also obtained

Circuit Simulations

Input and output matching using high impedance transmission lines for inductors and MIM capacitors added to circuit

S11 and S22 are improved above 10 GHz and upper band edge extended beyond 20 GHz

C2
C=0.28 pF

R
C7
C=5 pF

R
R4
R=200 Ohm

C
C10
C=10 pF

C
C3
C=10 pF

R
R1
R=20 Ohm

dB(S(2,2))
dB(S(1,1))

freq, GHz

dB(S(2,1))

freq, GHz

UCSB

MMIC Layout

RF Out

RF In

FET 2

FET 1

V_{G1} FET 2

V_{G2} FET 1 & 2

FET 1 DC Ground

2.65 mm

2.1 mm
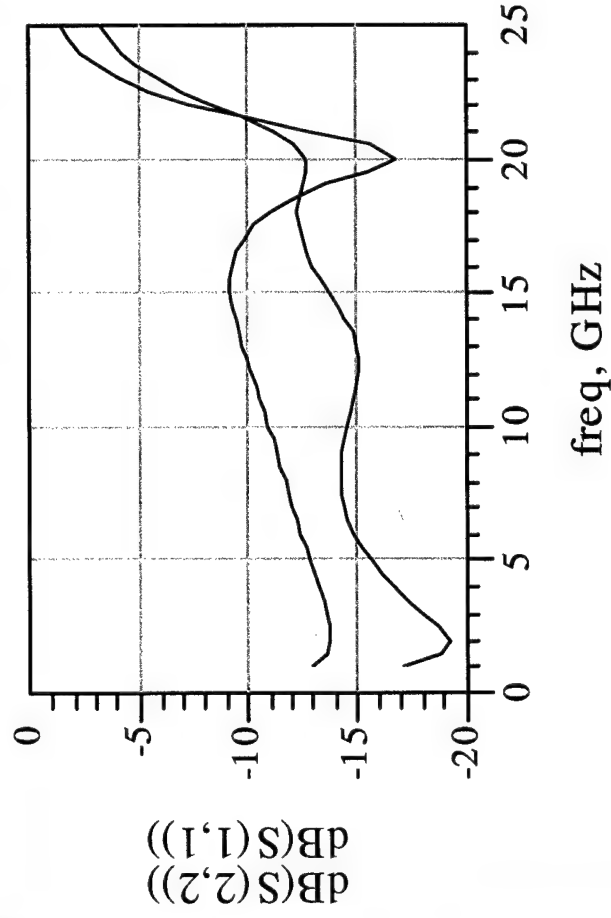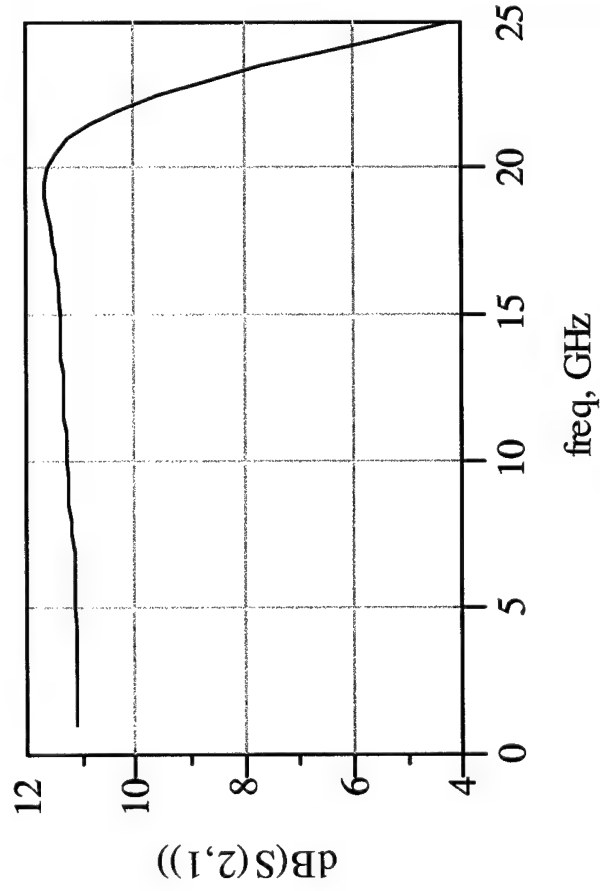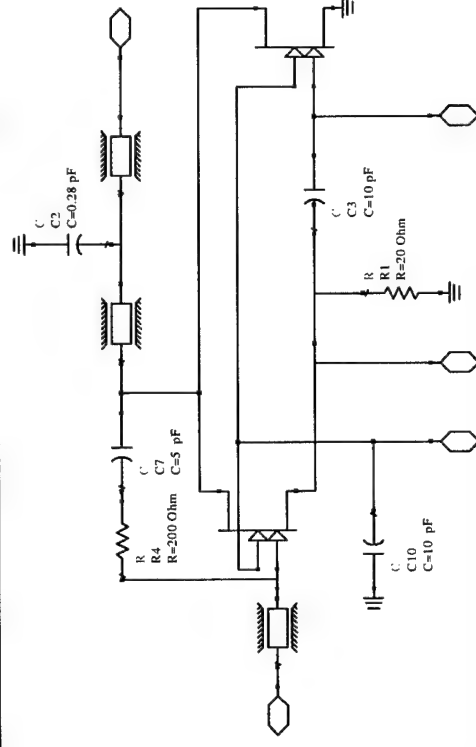
MMIC Process Flow

UCSB

Ohmic Layer: (Ti/Al/Ni/Au: 200/2000/550/450 A) RTA annealed

Mesa Isolation

NiCr Thin Film Resistors (50 Ω/□)
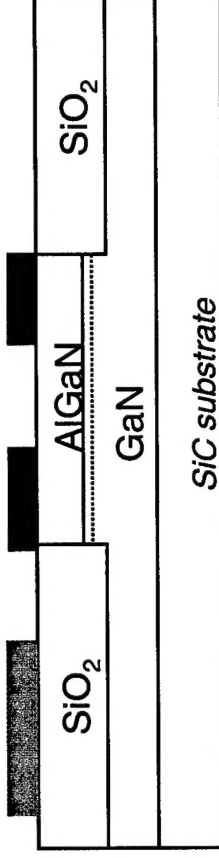
E-beam Gate Layer: Tri-layer resist process

Metal 1 Layer: Transmission lines, bottom of MIM capacitors
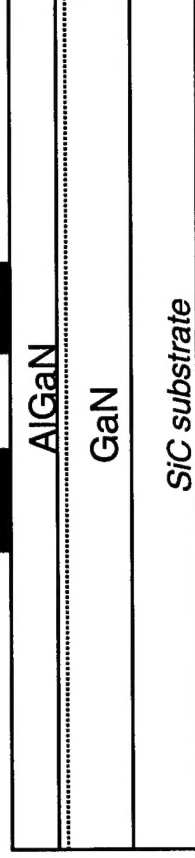
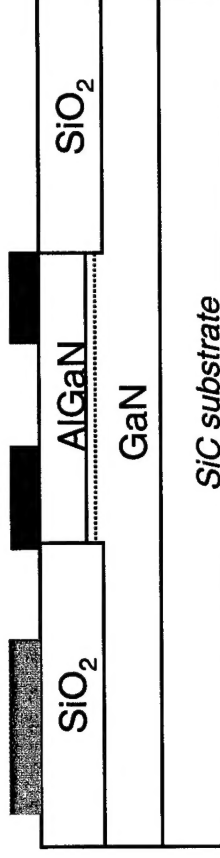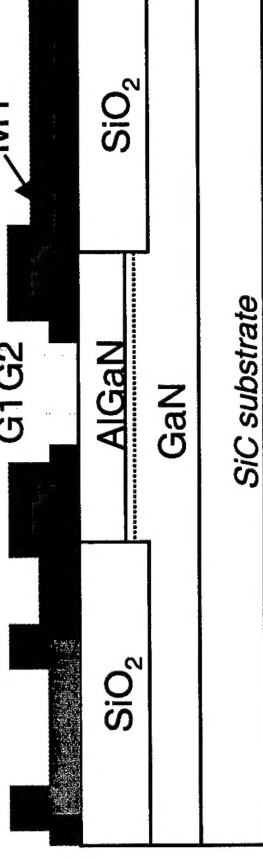# Process Flow

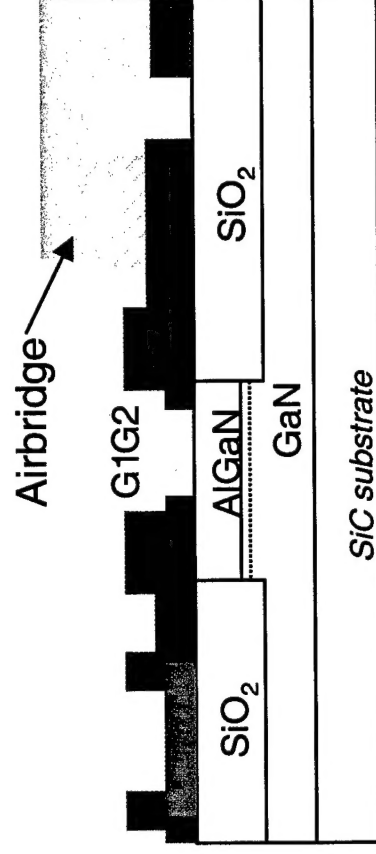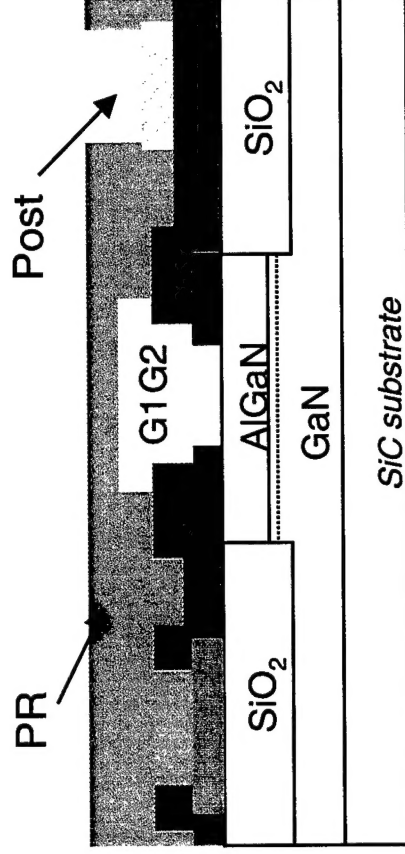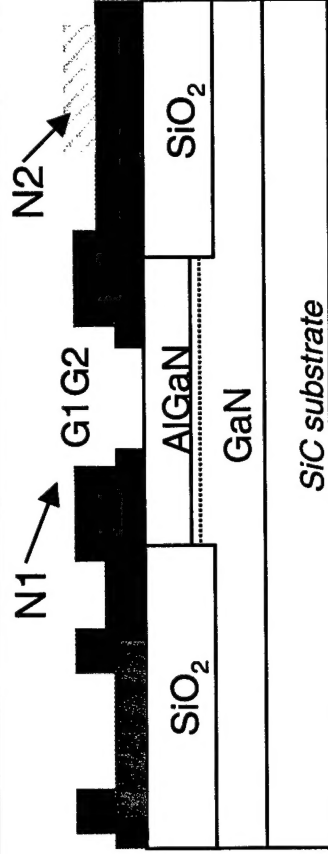# UCSB

Nitride 1 Layer (N1): Gate Passivation

Nitride 2 Layer (N2): Capacitor Dielectric

Airbridge Post layer

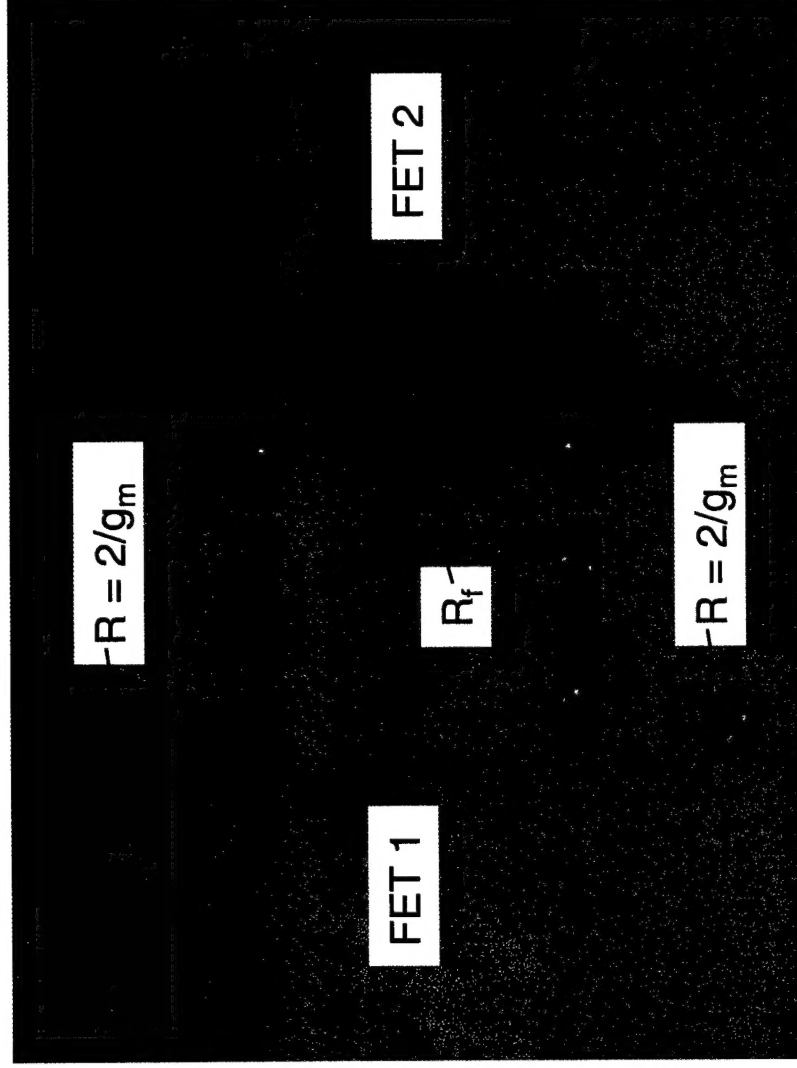Plated Airbridge

N2

N1

G1 G2

SiO₂

AlGaN

GaN

SiC substrate

SiO₂

Post

PR

G1 G2

SiO₂

AlGaN

GaN

SiC substrate

SiO₂

Airbridge

G1 G2

SiO₂

AlGaN

GaN

SiC substrate

SiO₂

Current Status

UCSB

Ohmic layer complete
Rougher morphology than usual
$R_c = 0.55\ \Omega mm$

Mesa isolation complete

NiCr resistor layer complete
$R_{sh} = 50\ \Omega/\square$

E-beam layer attempted, but
T-gates lifted completely
Rework in progress

1-18 GHz Dual gate GaN HEMT power amplifiers for Naval Radar

UCSB

Significance:
high current gain and high breakdown
sufficient bandwidth and power
for Navy 1-18 GHz, 2 W amplifier

Status
high ft dual gate GaN HEMTs demonstrated
ft-doubler with resistive feedback circuit designed

Future Plans
construct, test, power amplifiers

Expected Results
1-18 GHz amplifiers, 2-10 W output power

Alternatives
GaAs-based power PHEMTs

Navy and DOD Impact
1-18 GHz TWT drivers
power amplifier for AMRFS

Industry collaborations / transitions
Cree Lighting